AJNR

Standardized, Reproducible, High Resolution Global Measurements of T1 Relaxation Metrics in Cases of Multiple Sclerosis

Radhika Srinivasan, Roland Henry, Daniel Pelletier and Sarah Nelson

AJNR Am J Neuroradiol 2003, 24 (1) 58-67
http://www.ajnr.org/content/24/1/58

AJNR Am J Neuroradiol 24:58–67, January 2003

Standardized, Reproducible, High Resolution Global Measurements of T1 Relaxation Metrics in Cases of Multiple Sclerosis

Radhika Srinivasan, Roland Henry, Daniel Pelletier, and Sarah Nelson

BACKGROUND AND PURPOSE: **We herein present a methodology for standardized and clinically applicable measurement of T1 relaxation maps with high resolution and volumetric coverage by using the commercially available 3D spoiled gradient-echo sequence. The reproducibility of the T1 metrics derived from these maps and their sensitivity to distinguish between control participants and patients with multiple sclerosis are evaluated.**

METHODS: **Axial view 3D RF spoiled data sets with two flip angles were acquired at 1.5 T to generate the T1 maps, with all other imaging parameters (27/6 ms [TR/TE]; field of view, 180 × 240 × 186 mm^3; matrix, 192 × 256 × 124) kept identical between the two acquisitions. T1 maps were collected from 20 normal control participants and 32 patients with multiple sclerosis. An automated and operator-independent method was developed to segment the relaxation maps and define T1 metrics.**

RESULTS: **We showed that the metrics derived from these maps to represent tissue characteristics were highly reproducible (coefficient of variation, approximately 1% to 4%) and were significantly different between normal control participants and patients with multiple sclerosis ($P < .001$) for the small cohort of patients in this study.**

CONCLUSION: **The commercially accessible 3D spoiled gradient-echo sequence can be used to generate T1 relaxation maps with high resolution and volumetric coverage. The metrics derived from the relaxation maps are reproducible and have been shown to be sensitive to qualitative and quantitative differences between subgroups of patients with multiple sclerosis and control participants, with strong statistical significance. The use of a commercially available sequence enables the standardization and comparison of T1 metrics across different multiple sclerosis centers.**

MR relaxation parameters, T1 and T2, have been proposed as surrogate markers for disease progression in cases of multiple sclerosis and other degenerative diseases. Currently, MR imaging is used to identify focal lesions in cases of multiple sclerosis through intensity variations on T1- and T2-weighted images. Assessment of T1 nonenhancing hypointense multiple sclerosis lesions has been shown to provide stronger correlations with clinical markers of disability than standard T2-hyperintense lesions (1, 2). Histopathologic studies based on autopsy cases have shown that these chronic T1-hypointense lesions correspond to areas of axonal loss and gliosis (2). Recent studies have indicated that tissue that appears normal on conventional MR images is abnormal according to MR spectroscopy and magnetization transfer imaging (3–5). To completely understand the nature of multiple sclerosis, it is important to study normal appearing tissue in addition to lesions. To facilitate such an investigation, the technique used should provide accurate and reproducible tissue classification with high resolution that can be standardized across different MR imaging centers. Direct measurements of T1 provide an objective and standardized way to classify tissue. Segmentation techniques that use such relaxometric maps have been suggested as valuable tools for accurate, automated classification and absolute volume measurements (6–8).

Saturation recovery and inversion recovery se-

Received June 21, 2002; accepted after revision July 31.

This work was supported by grants from the National Institutes of Health (RO1 N539529-01A1 and K01 CA 076998) and the National Multiple Sclerosis Society (RG2655B6/1).

From the Magnetic Resonance Science Center (R.S., R.H., S.N.), the Department of Radiology, University of California, San Francisco and the University of California, San Francisco Multiple Sclerosis Center (D.P.), Department of Neurology, University of California, San Francisco, San Francisco, CA.

Address reprint requests to Radhika Srinivasan, PhD, Department of Radiology, Magnetic Resonance and Science Center, University of California, San Francisco, 1, Irving Street, AC 109, Box 1290, San Francisco, CA 94143.

quences are used most frequently to determine T1 values. These methods measure multiple points in the relaxation curve to compute T1 over a single section and involve prohibitively long imaging times because the largest TR should allow for a full recovery of longitudinal magnetization. Although these techniques provide ideal measurements of T1, they are not viable in most studies that require T1 values over a large region of interest within a reasonable imaging time. 2D multisection methods provide better coverage compared with single section measurements but are limited in the accuracy of their T1 values because of cross talk between individual sections and nonrectangular profiles for the different sections (9). Accurate T1 measurements with 2D multisection techniques can be made only with a correction for section profile imperfections (10, 11). Compared with 2D multisection techniques, 3D methods provide greater volume coverage at higher spatial resolution. Because 3D methods use a section nonselective pulse, they are less sensitive to section profile imperfections. Consequently, commercially available 3D sequences are expected to provide reasonable T1 measurements without algorithms to correct for pulse profiles. This is useful because the analytical form of the profile is not always disclosed by the vendors and it is difficult to standardize correction algorithms across centers.

Studies have used 2D multisection and 3D methods to estimate T1 by using spin-echo or gradient-echo images at two flip angles and/or TR (10–12). These studies have shown that estimates of T1 can be made with this approach. Reproducibility of T1 metrics is an important criterion for applications that use relaxation maps to track subtle changes that are not evident with clinical markers. Thus, the reproducibility of the algorithms used to determine correction factors for the relaxation maps should be examined.

In this study, we present a methodology to generate reproducible T1 maps with high resolution and volumetric coverage by using a commercially available 3D spoiled gradient-echo sequence. An automated and operator-independent method was developed to segment the relaxation maps and procedures for accurate calibration of the data examined. As an example of the application of this T1 mapping technique, we used metrics derived from such maps to examine disease characteristics from a cohort of patients with multiple sclerosis. The reproducibility of these T1 metrics and their sensitivity to distinguish between control participants and patients with multiple sclerosis is shown.

Methods

Data Acquisition

Axial view 3D RF spoiled data sets with two flip angles were acquired at 1.5 T to generate the T1 maps, with all other imaging parameters (27/6 ms [TR/TE]; field of view, 180 × 240 × 186 mm^3; matrix, 192 × 256 × 124) kept identical between the two acquisitions. The imaging time for this protocol depended on the spatial resolution desired. For this particular choice of imaging parameters, the imaging time to acquire the T1 map was 16 min. The position of the center of the coil relative to the landmark (at niason) was noted for each participant and patient. It was ensured that the excitation volume was centered on the corpus callosum.

Calculation of T1 Maps

The signal intensity from a spoiled gradient-echo imaging sequence with flip angle α is shown by equation. 1, assuming $TE << T2^*$ (10),

$$S = \frac{S_0(1 - f)\sin(\alpha)}{1 - \cos(\alpha) \cdot f} \quad 1)$$

where $f = \exp(-TR/T1)$ and S_0 is a constant describing the imager gain and proton attenuation. T1 maps were calculated by substituting the ratio of steady-state signal intensities obtained at two discrete flip angles into equation 1. The choice of the flip angles was based on minimizing the error estimate, $\delta T1/T1$ (Appendix A), for a range of T1 values.

Accuracy of T1 Estimates

We evaluated the accuracy of the T1 estimates obtained with the spoiled gradient-echo method by using the T1 measurements of the single section spin-echo saturation recovery as a standard. Phantoms were made with a range of T1 values by doping distilled water with different amounts of gadopentetate dimeglumine (Magnevist). The amount of Magnevist was computed so that the T1 values in these phantoms were in the range observed from the in vivo brain. The MR relaxation parameters for white matter, gray matter, and CSF in the in vivo brain at 1.5 T were 800, 900, and 4000 ms, respectively. The spin-echo T1 values of these phantoms were measured by fitting the relaxation curve obtained by using different TR values (TR = 350, 400, 500, 600, 800, 1000, 1500, 2000, 4000, 5000, 7000, 9000) over a single section. The in-plane resolution and thickness of the single section used for spin-echo measurements was kept identical with the spoiled gradient-echo acquisition used for the T1 measurements. The percent error ($= (T1_{SE} - T1_{spgr})/T1_{SE} \cdot 100$), where SE stands for spin-echo and spgr stands for spoiled gradient-echo, was computed for each T1 phantom. Subsequently, the in vivo accuracy of the two-point 3D spoiled gradient-echo method was estimated by imaging a control participant with the spin-echo and spoiled gradient-echo methods. Hereafter, the T1 values obtained with the spoiled gradient-echo method will be referred to as *estimates*.

Correction of T1 Estimates for RF Inhomogeneities

The transmitted RF field for the head coil is inhomogeneous for axial view section locations that are far from the coil center, particularly toward the inferior end of the coil (10). This inhomogeneity causes shifts in the estimated T1 values because of over and under flipping of the prescribed angle over the region of interest. To correct for inaccuracies caused by RF inhomogeneity, we adopted a procedure that was outlined in a report presented by Alfano et al (6). With this approach, the T1 histograms from each section are smoothed and the T1 scale factors needed to align the histograms from the different sections are calculated. These scale factors are then applied to the T1 maps. The effect of this inhomogeneity correction was examined on a phantom in the following way. A series of images was acquired along the longitudinal axis of the coil, and these images were used to estimate the T1 values. The uniformity of the T1 values along the superior-inferior axis of the coil was calculated by computing the percent deviation ($[T1 - T1_c]/T1_c \cdot 100$), where $T1_c$ is the estimated T1 value at the center of the coil. These images were then corrected for RF inhomogeneities by using the above procedure, and the uniformity was reassessed. Once this inhomogeneity correction was validated in this way, the relaxation maps of all data were corrected in a similar fashion before subsequent analysis.

Automated Tissue Segmentation with T1 Maps

Data were analyzed by using custom routines built with interactive data language software. A masking algorithm was used to extract the skull and CSF from the T1-weighted images before using these images to generate T1 maps. To extract the white matter distribution from the T1 map, the following procedure was adopted. A T1 value of 1000.0 was used to threshold the T1 map, and a contouring procedure was used to generate a white matter mask from this threshold image. The same threshold was used for all data sets in this study. In this algorithm, large gray matter structures and macroscopic lesions with T1 values greater than the predetermined threshold within the contour were assigned a negative value and extracted out of the mask. This white matter mask was applied to the T1 map to generate the white matter T1 distribution. As a result of the contouring procedure, some gray matter or lesions are included within this mask. To exclude these regions from the white matter volume, the T1 distribution was fit with a gaussian function and converted into a probability distribution of T1 values by using the gaussian probability density function. Based on this probability distribution, each pixel in the brain volume was assigned a probability based on its T1 value. The T1 range with a 90% probability was identified, and all pixels within this range were used to generate the white matter volume. This volume was classified as normal appearing white matter in patients. Pixels with a T1 value <0.9 and greater than the upper bound of the T1 range were segmented out into a second volume. This volume was classified as gray matter in normal control participants. In this procedure, the second volume included lesions for patients with multiple sclerosis. To obtain lesion-free gray matter volume, lesions were identified within the normal appearing white matter by using an automated contouring procedure with a T1/size threshold of 1200/5–1000 pixels. The lesions characterized in this way were removed from the gray matter volume before estimating its characteristics. The spatial locations of the segmented volumes were compared with the high resolution T1-weighted image for both normal control participants and patients with multiple sclerosis. These spatial locations were inspected by a neurologist to evaluate the accuracy of tissue classification.

Estimation of T1 Metrics

The location of the vermis was identified on the high resolution spoiled gradient-echo image as the most inferior section not including the cerebellum. The volume above this section was defined as the supratentorial brain volume and was used to derive the T1 parameters for all participants and patients. The T1 distributions of the segmented images were fit with a gaussian function to estimate the following metrics: the peak location and width of the white and gray matter, relative height (= height of white matter peak/height of gray matter peak), relative distance (= gray matter position − white matter position), and the white matter fraction (= volume of white matter/volume of the T1 map). Two-tailed Student's *t* test with unequal variance was used to estimate the statistical significance of differences in the T1 metrics between control participants and patients with multiple sclerosis.

Reproducibility of Metrics Derived from T1 Maps

Multiple T1 measurements were made for eight normal control participants to assess the in vivo reproducibility of T1 parameters. To allow for variability in participant position, participants either underwent imaging some days apart or were repositioned during the same session. The T1 maps from the multiple sessions were aligned to the first examination before segmenting the T1 maps to estimate the T1 metrics. The reproducibility of the metrics was assessed by computing the coefficient of variation.

TABLE 1: Study populations

Group	n (M/F)	Age (SD) (yr)	Disease Duration (yr)
Control	20 (9/11)	46.1 (9.3)	
RRMS	11 (4/7)	43.9 (11.5)	12.7 (8.9)
SPMS	13 (6/7)	49.7 (5.6)	16.5 (6.9)
PPMS	8 (4/4)	50.6 (3.6)	11.5 (6.5)
All patients with MS	32 (14/18)	47.9 (8.2)	13.8 (7.6)

Note.—M indicates male; F, female; RRMS, relapsing-remitting multiple sclerosis; SPMS, secondary progressive multiple sclerosis; PPMS, primary progressive multiple sclerosis; MS, multiple sclerosis. Relapsing-remitting multiple sclerosis and secondary progressive multiple sclerosis were defined by the Poser criteria (13). Primary progressive multiple sclerosis was defined by a progressive clinical worsening from onset for 12 months or more with no episode of acute neurologic exacerbation.

Patient Populations

The patient populations used for this study are outlined in Table 1. Patients with relapsing-remitting multiple sclerosis and patients with secondary progressive multiple sclerosis were defined by the Poser criteria (13). Patients with primary progressive multiple sclerosis were defined by a progressive clinical worsening from onset for $\geq$12 months with no episode of acute neurologic exacerbation. All patients with primary progressive multiple sclerosis had abnormal CSF, as defined by the presence of two or more oligoclonal bands or elevated immunoglobulin G index. All patients with multiple sclerosis were selected from a large group of patients followed by the University of California, San Francisco Multiple Sclerosis Center. The study was approved by the University of California, San Francisco Committee on Human Research, and all participants and patients provided informed written consent.

Results

Calculation of T1 Maps

We simulated the error estimate, $\delta T1/T1$ (Appendix A), for different combinations of two flip angles at a TR of 27 ms. These simulations indicated that the error estimate was minimized if the two flip angles were in the ranges of 35 to 45 degrees and 6 to 10 degrees. Considering this result, we chose to fix one of the flip angles at 40 degrees because it provided the most gray:white contrast and was consistent with the previous protocols. To determine the second flip angle, we simulated the error estimate, $\delta T1/T1$, with different combinations of two flip angles with one angle fixed at 40 degrees and the TR at 27 for phantoms with spin-echo values in the range of 600–1600 ms (Fig 1). It was observed that for low T1 values, the error estimate was minimized for flip angles between 6 and 8 degrees (Fig 1, *vertical solid lines*). For larger T1 values, the error was marginally greater at 8 degrees. Because the signal intensity-to-noise ratio increases with flip angle, we chose 8 degrees to be the second flip angle in our T1 calculations.

Accuracy of T1 Estimates

Figure 2A compares the T1 values from the spin-echo and spoiled gradient-echo methods for phantoms with spin-echo T1 values in the range of 400 to

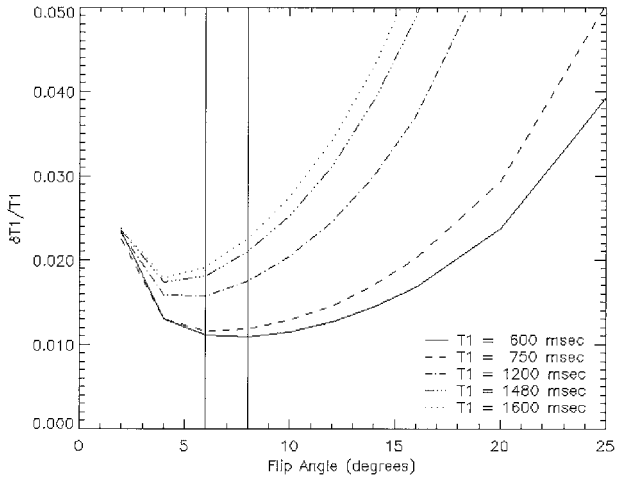

FIG 1. Error (δT1/T1) (Appendix A, equation 5) in using different combinations of two flip angles to estimate T1 values. One of the flip angles was fixed at 40 degrees, and a TR of 27 was used. *Vertical solid lines* indicate the flip angle range that minimizes the error for a T1 value of 600 ms.

1900 ms. Because we used the T1 values of the spin-echo technique as a standard, the *solid line* in this figure represents the ideal condition when the spoiled gradient-echo values are equal to the spin-echo T1 values. The *dashed line* in this figure shows the nonlinear function fit to the estimated T1 values obtained with the spoiled gradient-echo method. A mean percent shift of approximately 15% was observed in the T1 values of phantoms estimated with the spoiled gradient-echo method. Figure 2B compares the in vivo T1 values obtained with the spoiled gradient-echo and spin-echo techniques. In this T1 distribution, the highest peak corresponded to the location of white matter and the broader lower peak corresponded to the location of gray matter. This figure indicates that there was a 10% shift in the absolute values of the peak position of the white and gray matter. Figure 2 shows that the T1 values estimated from the spoiled gradient-echo method do differ systematically from those determined by the spin-echo method.

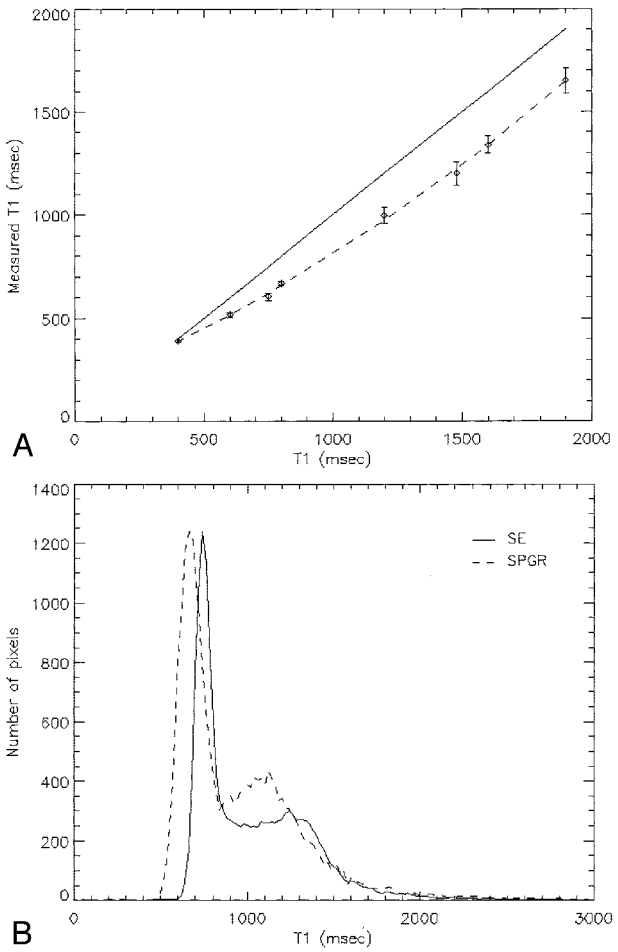

FIG 2. Comparison of T1 values from spin-echo and spoiled gradient-echo methods for phantom with spin-echo T1 values in the range of 400 to 1900 ms.

A, This figure shows the T1 estimate derived from the spoiled gradient-echo method (ordinate) for phantoms with different spin-echo T1 values (abscissa). The latter were used as the standard to evaluate the accuracy of the spoiled gradient-echo T1 values. *Points* are the mean T1 values of a region of interest from the respective phantoms, and *error bars* represent SD. *Solid line* represents the ideal situation when the spoiled gradient-echo values are equal to the spin-echo T1 values. *Dashed line* shows a nonlinear fit through the T1 values estimated with the spoiled gradient-echo method.

B, Comparison of the T1 distribution from a single section for a normal control participant using the spin-echo (*solid line*) and spoiled gradient-echo (*dashed line*) methods.

Correction of T1 Estimates for RF Inhomogeneities

The T1 estimates of a phantom along the longitudinal axis of the head coil with and without correction for RF inhomogeneity are displayed in Figure 3. Considering that the average distance between the landmark position at niason and the center of the coil was 3 cm and the size of the brain including the cerebellum is approximately 7 cm, the region of interest (ie, supratentorial brain volume) was contained within the homogeneous region of the head coil. The correction factors for RF inhomogeneity were relatively large for the inferior section locations (approximately 25%), compared with approximately 2% near the center of the coil.

Automated Tissue Segmentation with T1 Maps

The procedure used to extract white matter and normal appearing white matter from the T1 maps of study participants and patients is outlined in Fig 4. A T1 value of 1000.0 was used to threshold the T1 map (Fig 4A), and a contouring procedure was used to generate a white matter mask from this threshold image (Fig 4B). The mask is applied to the T1 map to generate a T1 distribution (Fig 4C, *solid line*), which is fit to a Gaussian function (Fig 4C, *dot-dashed line*) and converted into a probability distribution of T1 values. All pixels with T1 values within 90% probability (Fig 4C, *vertical dashed line*) are used to generate the white matter volume (Fig 4D). The results of

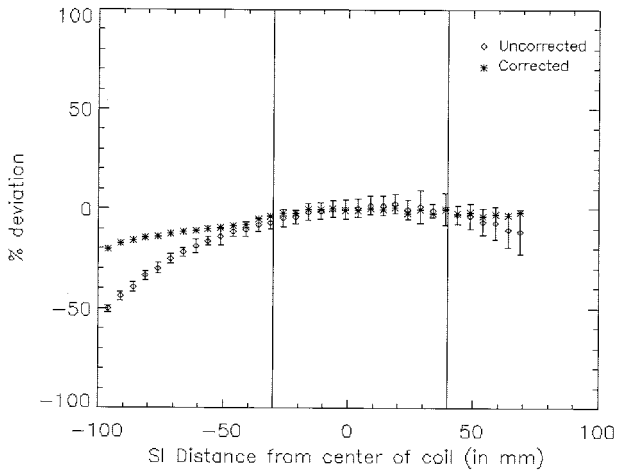

FIG 3. Percent deviation of T1 estimates from uniformity along the superior-inferior direction for uncorrected and corrected data. Negative values on the abscissa correspond to inferior section locations. The data were corrected for RF inhomogeneity by using a procedure outlined by Alfano et al (6). Considering that the average distance between the landmark position at niason and the center of the coil was 3 cm and that the size of the brain including the cerebellum is approximately 7 cm, the region of interest (ie, supratentorial brain volume) was contained within the homogeneous region of the head coil (*solid lines*).

the T1 mapping and segmentation technique are shown in Fig 5 for a control participant (*upper panel*) and a patient with relapsing-remitting multiple sclerosis (*lower panel*). The T1 map (Fig 5B) correlates well with the T1-weighted image (Fig 5A) both for control participants and patients. Regions with large T1 values that have low intensity on T1-weighted images are bright on the T1 map. The same section is shown segmented into white matter (classified as normal appearing white matter in patients) (Fig 5C) and gray matter (Fig 5D). The white matter regions identified by the segmentation procedure correlated well with the T1-weighted image contrast that was used to differentiate white and gray matter regions on T1-weighted images. In addition, multiple sclerosis lesions, seen as hypointensities on T1-weighted images, were effectively excluded from either of the segmented volumes. The segmented images were inspected by a neurologist, and it was determined that the automated and operator-independent procedure accurately classified the respective volumes. It was also noted that the lesion identification procedure, based on using a T1 threshold value, resulted in false positives from gray matter regions within the normal appearing white matter. The gray matter volume also includes some residual CSF regions in the sulci that are not removed by the masking procedure.

Estimation of T1 Metrics

Figure 6 displays the T1 distribution for a participant. The distribution is segmented into white (*dashed line*) and gray (*dot-dashed line*) matter volumes by using the gaussian distribution. The respective distributions correspond well to the overall T1 distribution (*solid line*). The *vertical lines* in this figure indicate the T1 range used to segment the white matter volume. The T1 metrics for the white and gray matter were derived from the respective gaussian fits.

Reproducibility of T1 Metrics

Figure 7 examines the in vivo reproducibility of the technique from the T1 distributions of a control participant obtained during two different sessions. The shape and locations of the peak positions of the two distributions were reproducible. The coefficient of variation of the white and gray matter peak positions was approximately 1% (Table 2). The coefficient of variation of the remaining T1 metrics was within 4%. Although the T1 values of the spoiled gradient-echo method were not directly equivalent to the spin-echo measurements, Figure 7 and Table 2 illustrate that the T1 metrics derived from the relaxation maps and segmentation procedure were reproducible.

Comparison of T1 Metrics between Control Participants and Patients with Multiple Sclerosis

Table 3 compares the average T1 distributions between control participants and all multiple sclerosis populations. The location and width of the white matter distribution in patients with multiple sclerosis increased by approximately 8% ($P < .001$) and 18% ($P < .001$), respectively. The relative distance between the white and gray matter peak positions decreased in patients relative to control participants by approximately 10% ($P < .001$). The statistical significance of these results is maintained when a patient subgroup (relapsing-remitting multiple sclerosis, secondary progressive multiple sclerosis) is compared with the control group (Table 3). Figure 8 compares the average T1 histogram between control participants and the different multiple sclerosis subgroups. These histograms were pooled from all the participants and patients in the respective populations outlined in Table 1. Visual inspection of this figure indicates that the peaks are not as well differentiated for patients as for control participants. Considering these results, we conclude that the T1 distributions obtained from the spoiled gradient-echo method are sensitive to qualitative and quantitative differences between control participants and patients with multiple sclerosis.

Discussion

Changes in biochemical processes caused by disease are reflected through modified MR relaxometric parameters. T1- and T2-weighted images are often used to make qualitative evaluations of disease status and have been proposed by some centers for quantitative analysis. The contrast in such sequences arises from a combination of factors that often depend on both the physical and imaging parameters used. Hence, it is difficult to compare quantitative measurements between different institutions, imagers, and software platforms. Relaxometric parameters

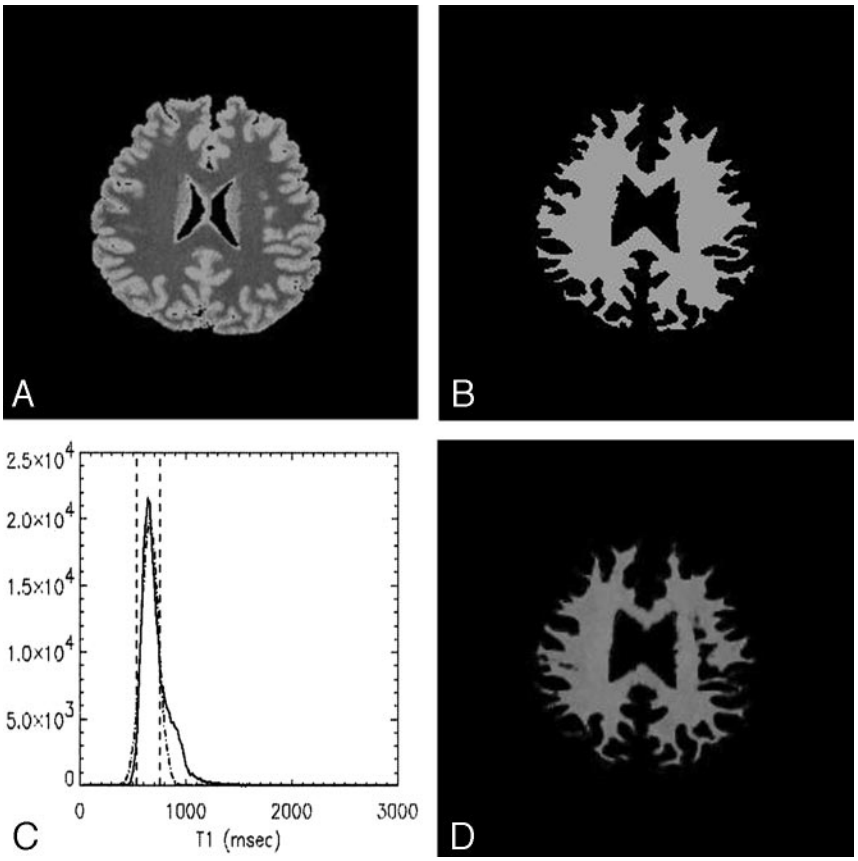

FIG 4. Procedure used to extract white matter and normal appearing white matter from T1 maps of study participants and patients.

A, T1 value of 1000.0 is used to threshold the T1 map.

B, White matter masks obtained by contouring the threshold T1 map.

C, The T1 distribution (*solid line*) obtained by applying the mask in *B* to the map in *A*. This distribution is fit to a Gaussian function (*dot-dashed line*) and converted into a probability distribution of T1 values.

D, White matter volume obtained by extracting pixels with T1 values within 90% probability (*vertical lines* in *C*).

provide an absolute measure of underlying disease activity and are likely to be more accurate measures of the effects of disease progression. In this study, T1 maps were generated with high resolution and volumetric coverage. These maps had good signal intensity-to-noise ratios and a dynamic range of T1 values.

The results of the optimization procedure that was used to determine the two flip angles for T1 measurements were consistent with previous results (14) and results of other two-point methods (12). With gradient-echo methods, the error in the T1 estimate depends on the range of flip angles and TR used (15). The optimization procedure should be repeated for a different set of desired parameters and imagers and after system upgrades. The in vivo T1 estimates for different regions of the brain are similar to values reported for these regions in other studies (10). One of the causes for the systematic deviation of T1 values between gradient-echo and saturation recovery methods arises from the assumption in equation 1 that there is zero residual magnetization at the time of each sampling pulse (15). Although this is true if $TR \gg T2^*$, this is not the case for most clinical sequences used for in vivo studies. Also, because the phantoms have a relatively long T2, the discrepancy between the variable flip angle and saturation recovery is expected to be greater for phantoms than for biologic tissue, as seen in this study. To correct for these factors, a calibration curve, such as the one shown in Figure 2, should be measured at different institutions and across software and hardware upgrades by using a standard phantom. This would enable a comparison of the different T1 mapping techniques and would provide a reference to ensure the stability of the technique over time.

T1 mapping methods that use multisection 2D images are affected by inaccuracies in section-selective pulse profiles to a greater extent than are 3D techniques. Uncorrected T1 estimates with 2D methods deviate more significantly from their "true" T1 values compared with 3D acquisition. As seen from this study, the deviation of T1 values is approximately 10% across a range of T1 values compared with a 2D acquisition, with which the uncorrected T1 values deviate by as much as 50% (10). Because the central sections of a 3D volume are expected to have a rectangular profile, placing the region of interest at the center, as in this study, provides reasonably accurate T1 estimates.

Both 2D and 3D acquisitions suffer from B1 field inhomogeneities, which cause a nonuniformity of the estimated T1 values. If the B1 field were uniform, all partitions within the region of interest would experience the same excitation profile at the prescribed flip angle. For the head coil, the transmitted field is nonuniform toward the edges of the field of view. This causes spatial variations in the flip angle across the transverse plane and thickness of the section, which results in nonuniformity of the estimated T1 values. The receive fields in two-point methods are relatively insensitive to B1 inhomogeneities because the ratio of signal intensities is used rather than a single intensity

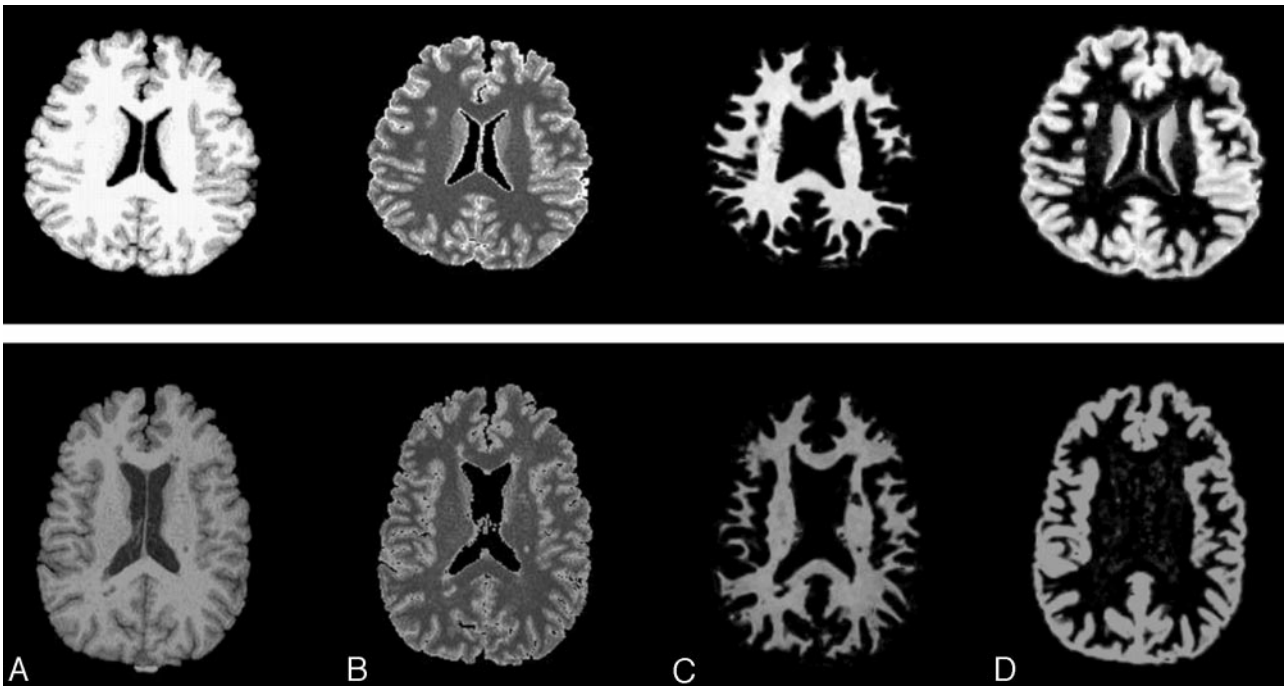

FIG 5. Results of the T1 map calculation and segmentation procedure from a normal control participant (*upper panel*) and a patient with relapsing-remitting multiple sclerosis (*lower panel*).
A, T1-weighted images.
B, T1 maps.
C, Segmentation into white matter.
D, Segmentation into gray matter.

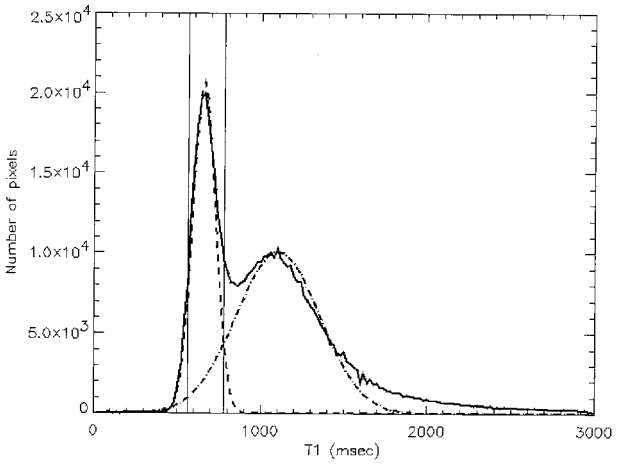

FIG 6. T1 distribution for a normal control participant (*solid line*), segmented into white matter (*dashed line*) and gray matter (*dot-dashed line*) components. *Vertical solid lines* represent the T1 range used to generate the white matter volume.

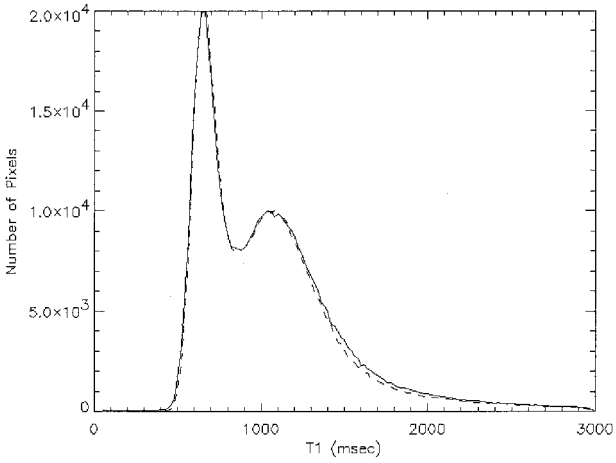

FIG 7. Reproducibility of T1 measurements. T1 distribution for one control participant who underwent imaging multiple times with the 3D spoiled gradient-echo method. *Solid line*, session 1; *dashed line*, session 2.

value. Although the T1 maps in this study were corrected for RF field inhomogeneity, it was observed that the correction factors were not very significant (approximately 2%) within the region of interest. Based on the relative distance between the landmark and the center of the coil, we found that supratentorial volume, used to estimate T1 metrics, was always within the homogeneous region of the coil as defined by the *solid lines* in Figure 3.

Several techniques have been used to segment brain tissue and identify lesions. Most of these techniques use signal intensity MR data (16, 17). These methods are susceptible to irreproducible tissue registration because of variations in contrast from different MR imagers or imaging parameters (18, 19) and are influenced by RF inhomogeneity to a greater extent than are relaxation maps (6). Previous studies have shown that metrics derived from signal intensity

TABLE 2: Coefficient of variation of the T1 metrics obtained from multiple T1 measurements from eight normal control participants

n = 8	White Matter		Gray Matter		Relative Height	Relative Distance	White Matter Fraction
	Position	Width	Position	Width			
Coefficient of variation	1.0	3.8	1.1	3.2	2.7	2.5	3.9

Note.—The metrics computed were white matter and gray matter peak positions and widths, relative height (height of white matter/height of gray matter), and relative distance (gray matter position − white matter position).

TABLE 3: Comparison of T1 metrics between control participants and patients with multiple sclerosis

	White Matter		Gray Matter		Relative Height	Relative Distance
	Position	Width	Position	Width		
Control participants	667	70	1077	233	2.26	409
All patients with MS	722	83	1090	207	2.05	367
P values	<0.001	<0.001	0.33	<0.001	0.003	<0.001
RRMS and SPMS	714	79	1088	212	2.02	373
P values	<0.001	0.001	0.38	0.002	0.002	<0.001

Note.—The two-tailed Student's *t* test with unequal variance is used to derive statistical significances (*P* values). MS, multiple sclerosis; RRMS, relapsing-remitting multiple sclerosis; SPMS, secondary progressive multiple sclerosis.

information alone do not offer good reproducibility (20). Recent studies (21) have shown that reproducible brain tissue volume measurements can be derived from a statistical parametric matching (SPM)-based segmentation methodology with which both spatial prior probabilities (22) and signal intensity information are used. We have presented an automated, operator-independent segmentation procedure that uses T1 relaxation maps to generate tissue volumes. The use of T1 relaxation values rather than T1-weighted intensity to identify tissue type allows for a procedure that uses absolute T1 cutoffs, which remain invariant between different participants because they are independent of underlying intensity variations. Unlike the procedure outlined in a report presented by Alfano et al (6), this segmentation algorithm does not require user input to generate preclassified regions of interest. The segmented gray matter volume includes residual CSF in the sulci surrounding the gray matter regions. The gray matter location and width are not influenced by these CSF regions because the gaussian function used to estimate these metrics does not fit the tail of the distribution.

For in vivo studies, visual inspection by a neurologist verified that the segmentation procedure classified the tissues appropriately. Although the segmentation procedure was considered accurate to examine global properties, tissue classification should be validated by using anatomic information by normalizing participant data with a standard atlas, such as the Talairach atlas, before regional properties of the T1 maps can be examined.

The small coefficient of variation (approximately 1% to 4%) in the T1 metrics shows the high degree of reproducibility of the relaxation maps and the segmentation technique. The extent of reproducibility for the white matter fraction was similar to that in other reported studies (21) for a comparable control population. This degree of reproducibility in the T1 metrics enhances the sensitivity of detection of small disease-related changes and is suitable for longitudinal studies. The locations of peak positions are significant indicators of disease status. These metrics cannot be derived from techniques that use signal intensity MR data because they do not provide reproducible peak locations.

In the segmentation procedure presented herein, the white matter distribution was selected the same way for patients and for control participants. This fixed the definition of "white" matter for patients relative to control participants. Any normal appearing white matter changes could therefore be directly compared with control data. The widening and shifting of the normal appearing white matter peak location and decrease in the relative distance between the white and gray matter peaks evident from our results suggested an increase in T1 values with disease. For the relatively small cohort of patients in this study, a strong statistically significant difference was seen between patients and control participants for the position and width of the white matter peak and also for the relative distance between the peak locations. The gray matter location was not significantly different between control participants and patients (Table 3), compared with the differences in the white matter position, which indicated that the normal appearing white matter T1 values were shifting toward larger values, typically seen for gray matter. The statistical significance of these results was maintained even for a subset of patients (relapsing-remitting multiple sclerosis, secondary progressive multiple sclerosis), showing the strength of these results. This also suggests that the results were not driven by patients with primary progressive multiple sclerosis, which is thought to be a different clinical subtype. The gradual shift in the T1 values of the normal appearing white matter toward higher values also explains the loss of differentiation between the white and gray matter locations in patients with multiple sclerosis (Fig 8).

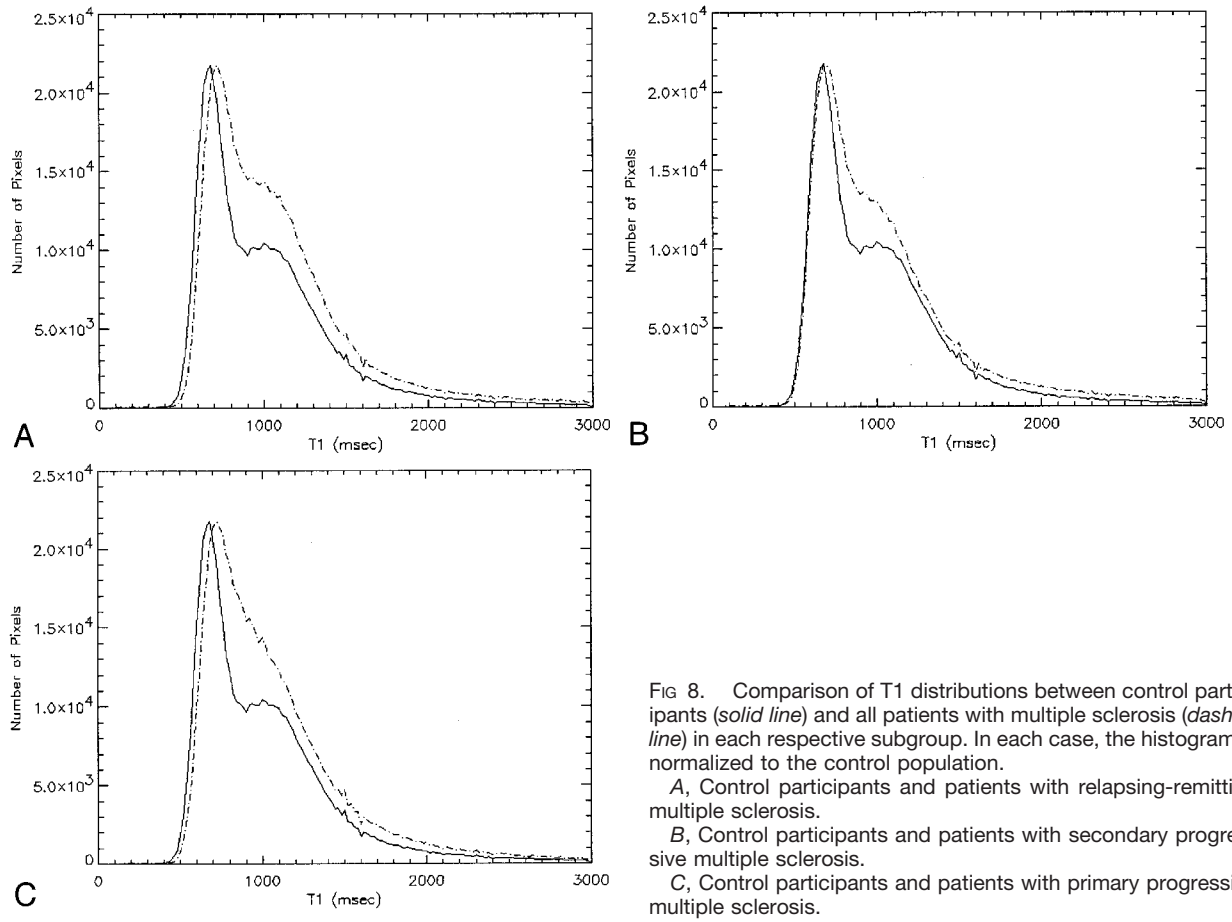

FIG 8. Comparison of T1 distributions between control participants (*solid line*) and all patients with multiple sclerosis (*dashed line*) in each respective subgroup. In each case, the histogram is normalized to the control population.

A, Control participants and patients with relapsing-remitting multiple sclerosis.

B, Control participants and patients with secondary progressive multiple sclerosis.

C, Control participants and patients with primary progressive multiple sclerosis.

The segmentation procedure outlined herein provides an estimate of the normal appearing white matter without visible multiple sclerosis lesions. However, identification of lesions based on their T1 values alone erroneously removes some gray matter regions. For this reason, the nature of differences in gray matter between control participants and patients, although promising, needs to be further investigated. Accurate automated lesion volume calculations using T1 relaxation values will therefore require a multispectral approach (7). In this study, the gray matter fraction was not computed because the CSF was not adequately removed; this could affect the gray matter volume measurements.

Most clinical multiple sclerosis imaging protocols already acquire proton density, T2- and T1-weighted data sets to qualify brain atrophy and lesion load. Because T1 relaxation maps are generated using T1-weighted images, the T1 mapping technique presented here can be easily incorporated into the protocol. The use of a commercially available sequence to generate T1 maps will facilitate the computation of valuable T1-related metrics that can be readily standardized and compared across multiple sclerosis centers. Although the application of the T1 mapping technique to cases of multiple sclerosis has been presented in this study, this method can be used to examine the disease characteristics of different pathologic abnormalities.

Future work will involve using this technique to quantify focal and global tissue changes in patients with multiple sclerosis, both across the different subgroups and longitudinally. The results from white and gray matter maps were promising and will lead us to study normal appearing white matter and gray matter changes in a larger cohort of patients with multiple sclerosis. The fluid-attenuated inversion recovery acquisition will be used to adequately remove CSF and quantify gray matter volume. The diseased volume, identified based on T1 differences between control participants and patients, will be correlated with other imaging modalities, such as magnetization transfer and diffusion tensor imaging.

Conclusion

The 3D spoiled gradient-echo method with two flip angles can be used to generate T1 relaxation maps with high resolution and volumetric coverage. The T1 metrics derived from these maps are highly reproducible (coefficient of variation, approximately 1% to 4%). This is a strong result because it incorporates measurement, biologic, and inter- and intra-participant variability. The metrics derived from the relaxation maps are shown to be sensitive to qualitative and quantitative differences between multiple sclerosis patient subgroups and control participants, with strong statistical significance ($P < .001$). The use of a

commercially available sequence enables the standardization and comparison of T1 metrics across different multiple sclerosis centers.

Appendix

The signal intensity from a spoiled gradient-echo imaging sequence with flip angle α is given by equation 2, assuming $TE << T2^*$ (10):

$$S = \frac{S_0(1 - f)\sin(\alpha)}{1 - \cos(\alpha) \cdot f} \quad (2)$$

where $f = \exp(-TR/T1)$ and S_0 is a constant describing the imager gain and proton attenuation. If S_1 and S_2 are the steady-state signal intensities obtained by using flip angles α_1 and α_2, the ratio of their signal intensities is given as follows.

$$R = \frac{S_1}{S_2} = \frac{\sin(\alpha_1)}{\sin(\alpha_2)} \cdot \frac{(1 - \cos(\alpha_2) \cdot f)}{(1 - \cos(\alpha_1) \cdot f)} \quad (3)$$

Specifically, if the ratio of signal intensities $R = S_1/S_2$ is used to derive T1 values, the noise in the T1 estimate is given as follows (11).

$$\delta T1 = (\partial T1/\partial R)(\delta R) \quad (4)$$

Here, $\partial T1/\partial R$ is derived from equation 3, and the noise in the ratio, δR, is given as follows.

$$\delta R = \{[(\delta S/\sqrt{N_1})/S_1]^2 + [(\delta S/\sqrt{N_2})/S_2]^2\}^{0.5} R \quad (5)$$

N_1 and N_2 are the number of data averages used to obtain images S_1 and S_2. To determine $\delta T1$ experimentally, data were collected on phantoms with different combinations of two flip angles, with one flip angle fixed at 40 degrees and the TR fixed at 27. Equation 4 was used to compute the error in the T1 value obtained with the spoiled gradient-echo technique. To measure δS, two data sets were acquired on the T1 phantoms with identical imaging parameters but with different numbers of averages (two and four). A ratio image was formed from these images, and noise, δS, was computed as the SD of pixels within each T1 phantom.

References

1. Filippi M, Horsfield MA, Tofts PS, Barkhof F, Thompson AJ, Miller DH. **Quantitative assessment of MRI lesion load in monitoring the evolution of multiple sclerosis.** *Brain* 1995;118:1601–1612
2. van Walderween MA, Barkhof F, Hommes OR, et al. **Correlating MRI and clinical disease activity in multiple sclerosis: relevance of hypointense lesions on short-TR/short-TE (T1-weighted) spin-echo images.** *Neurology* 1995;45:1684–1690
3. Fu L, Matthews PM, De Stefano N, et al. **Imaging axonal damage of normal-appearing white matter in multiple sclerosis.** *Brain* 1998; 121:103–113
4. Tortorella C, Viti B, Bozzali M, et al. **A magnetization transfer histogram study of normal-appearing brain tissue in MS.** *Neurology* 2000;54:186–193
5. Sharma R, Narayana PA, Wolinsky JS. **Grey matter abnormalities in multiple sclerosis: proton magnetic resonance imaging.** *Mult Scler* 2001;7:221–226
6. Alfano B, Brunetti A, Covelli EM. **Unsupervised, automated segmentation of the normal brain using a multispectral relaxometric MR approach.** *Magn Reson Med* 1997;37:84–93
7. Alfano B, Brunetti A, Larobina M, et al. **Automated segmentation and measurement of global white matter lesion volume in patients with multiple sclerosis.** *J Magn Reson Imaging* 2000;12:799–807
8. Vinitski S, Gonzalez C, Mohamed F. **Improved intracranial lesion characterization by tissue segmentation based on a 3D feature map.** *Magn Reson Med* 1997;37:457–469
9. Hanicke W, Merboldt K-D, Frahm J. **Slice selection and T1 contrast in FLASH NMR imaging.** *J Magn Reson* 1988;77:64–74
10. Parker GJ, Barker GJ, Tofts PS. **Accurate multislice gradient echo T1 measurement in the presence of non-ideal RF pulse shape and RF field homogeneity.** *Magn Reson Med* 2001;45:838–845
11. Prato FS, Drost DJ, Keys T, Laxon P, Comissiong B, Sestini E. **Optimization of signal-to-noise ratio in calculated T1 images derived from two spin-echo images.** *Magn Reson Med* 1986;3:63–75
12. Brookes JA, Redpath TW, Gilbert FJ, Needham G, Murray AD. **Measurement of spin-lattice relaxation times with FLASH for dynamic MRI of the breast.** *Br J Radiol* 1996;69:206–214
13. Poser CM, Paty DW, Scheinberg L, McDonald WI, Davis FA, Ebers GC. **New diagnostic criteria for multiple sclerosis: guidelines for research protocols.** *Ann Neurol* 1983;13:227–231
14. Filippi M, Rocca MA, Horsfield MA, et al. **Increased spatial resolution using a three-dimensional T1-weighted gradient-echo MR sequence results in greater hypointense lesion volumes in multiple sclerosis.** *AJNR Am J Neuroradiol* 1998;19:235–238
15. Imran J, Langevin F, Saint-Jalmes H. **Two-point method for T1 estimation with optimized gradient-echo sequence.** *Magn Reson Imaging* 1999;17:1347–1356
16. Fram EV, Herfkens RJ, Johnson, GA, et al. **Rapid calculation of T1 using variable flip angle gradient refocused imaging.** *Magn Reson Imaging* 1987;5:201–208
17. Rovaris M, Inglese M, Schijndel RA, et al. **Sensitivity and reproducibility of volume change measurements of different brain portions on magnetic resonance imaging in patients with multiple sclerosis.** *J Neurol* 2000;247:960–965
18. Jackson EF, Narayana PA, Falconer JC. **Reproducibility of nonparametric feature map segmentation for determination of normal human intra-cranial volumes using MR imaging data.** *J Magn Reson Imaging* 1994;4:692–700
19. Harris GJ, Barta PE, Peng LW. **MR volume segmentation of gray matter and white matter using manual thresholding: dependence on image brightness.** *AJNR Am J Neuroradiol* 1994;15:225–230
20. Narayana PA, Borthakur A. **Effect of radio frequency inhomogeneity correction on the reproducibility of intra-cranial volumes using MR image data.** *Magn Reson Med* 1995;33:396–400
21. Chard DT, Parker GJ, Griffin CM, Thompson AJ, Miller DH. **The reproducibility and sensitivity of brain tissue volume measurements derived from an SPM-based segmentation methodology.** *J Magn Reson Imaging* 2002;15:259–267
22. Ashburner J, Friston KJ. **Voxel-based morphometry: the methods.** *Neuroimage* 2000;11:805–821